Paek, Min-Kyu; Jeon, Junmo; Lindberg, Daniel

Thermodynamic behaviour of nitrogen in the carbon saturated Fe-Mn-Si alloy during casting

Published in:
International Journal of Cast Metals Research

DOI:
10.1080/13640461.2020.1834176

Published: 02/09/2020

Document Version
Publisher's PDF, also known as Version of record

International Journal of Cast Metals Research

ISSN: (Print) (Online) Journal homepage: www.tandfonline.com/journals/ycmr20

Thermodynamic behaviour of nitrogen in the carbon saturated Fe-Mn-Si alloy during casting

Min-Kyu Paek, Junmo Jeon & Daniel Lindberg

To cite this article: Min-Kyu Paek, Junmo Jeon & Daniel Lindberg (2020) Thermodynamic behaviour of nitrogen in the carbon saturated Fe-Mn-Si alloy during casting, International Journal of Cast Metals Research, 33:4-5, 226-232, DOI: 10.1080/13640461.2020.1834176

To link to this article: https://doi.org/10.1080/13640461.2020.1834176

Published online: 15 Oct 2020.

INTERNATIONAL JOURNAL OF CAST METALS RESEARCH
2020, VOL. 33, NOS. 4–5, 226–232
https://doi.org/10.1080/13640461.2020.1834176

Taylor & Francis
Taylor & Francis Group

Thermodynamic behaviour of nitrogen in the carbon saturated Fe-Mn-Si alloy during casting

Min-Kyu Paek, Junmo Jeon and Daniel Lindberg

Department of Chemical and Metallurgical Engineering, Aalto University, Espoo, Finland

ABSTRACT

The evolution of nitrogen gas formation in cast iron was studied based on the information of the N solubility in the carbon-saturated iron-containing Mn and Si over the wide temperature range. In order to verify the accuracy of the Fe-Mn-Si-C phase diagram, the transition temperatures of the Fe-Mn-2.7 wt%Si-C_{sat} alloys were measured according to the Mn concentration using a differential scanning calorimetry under the purified Ar atmosphere. The recent thermodynamic modelling result of the Fe-Mn-Si-C-N system was used to describe the solubility limit of N in liquid and solid solution in the carbon saturated iron alloys. The cooling and quenching experiments were also carried out to check the effects of temperature and phase transformation on the N solubility limit in the temperature range from 500°C to 900°C.

ARTICLE HISTORY
Received 31 October 2019
Accepted 3 October 2020

KEYWORDS
Nitrogen; defect; blowholes; grey cast iron; transition temperature; Fe-Mn-Si -C-N system

Introduction

Nitrogen blowholes are the typical surface defects of grey cast iron. Since these perpendicular holes can be discovered at the most expensive machining stage, the major cost for the foundry has been a scrap of the defective cast irons. Even though the defects have been controlled by the blending of high purity raw materials, the fundamental solution has not been discussed until now. In this alloy grade, Si can be added up to 3 wt% for destabilising the iron carbide, and Mn can also be added to remove the detrimental effect of S in the cast iron [1,2]. Si is well known to decrease the C and N solubility, whereas Mn increases them in liquid iron. In addition, C has a significantly strong repulsion force with N in liquid iron [3]. Such complex relation among Mn, Si, C and N in cast iron has been recently described only for the liquid iron alloys. Therefore, in order to control the evolution of N_2 gas during solidification of grey cast iron, thermodynamic interactions among the alloying and gaseous impurity elements in the Fe-Mn-Si -C-N system have to be understood over the entire temperature range from the process condition to the room temperature.

In the authors' recent study [4], the N solubility in C saturated iron melts was measured in the temperature range from 1300°C to 1600°C. Using the Wagner's interaction parameter formalism [5], the first- and second-order interaction parameters among Mn, Si, C and N in liquid iron alloys were determined based on the N solubility data measured in the C saturated liquid iron containing Si and Mn. The experimental data of N solubility in Fe-C_{sat}, Fe-Si-C_{sat} and Fe-Mn-C_{sat} melts were reproduced well with the determined interaction parameters. However, as shown by the dashed line in Figure 1, the prediction with the first- and second-order parameters shows the more significant deviation with increasing temperature in the multicomponent Fe-Mn-Si-C_{sat}-N alloy containing 1.9 wt%Mn and 2 wt%Si. Although the accuracy can be improved by introducing the third-order interaction parameter of N, it has not been tried due to the absence of a definition for the higher-order parameter in the reciprocal relationship of Wagner's formalism [6].

In order to resolve the limitation of Wagner's formalism, the liquid solution property has been thermodynamically modelled using Modified Quasichemical Model (MQM) by the authors' recent study [7]. The N dissolution in the liquid Fe-Mn-Al-Si-C and its subsystems has been successfully reproduced using only binary MQM parameters, because MQM can intrinsically treat the strong interaction between alloying elements by adopting the pair exchange reaction. The calculated N solubility with temperature was shown as the solid line in Figure 1. Compared to the prediction by Wagner's formalism, the predictability of N solubility was improved over the wide range of melt temperatures without any additional parameter in the multicomponent system. This modelling result was adopted in this study for the calculation of N solubility change in the liquid alloys during cooling.

CONTACT Min-Kyu Paek min.paek@aalto.fi Department of Chemical and Metallurgical Engineering, Aalto University, Espoo, Finland

This article has been republished with minor changes. These changes do not impact the academic content of the article.

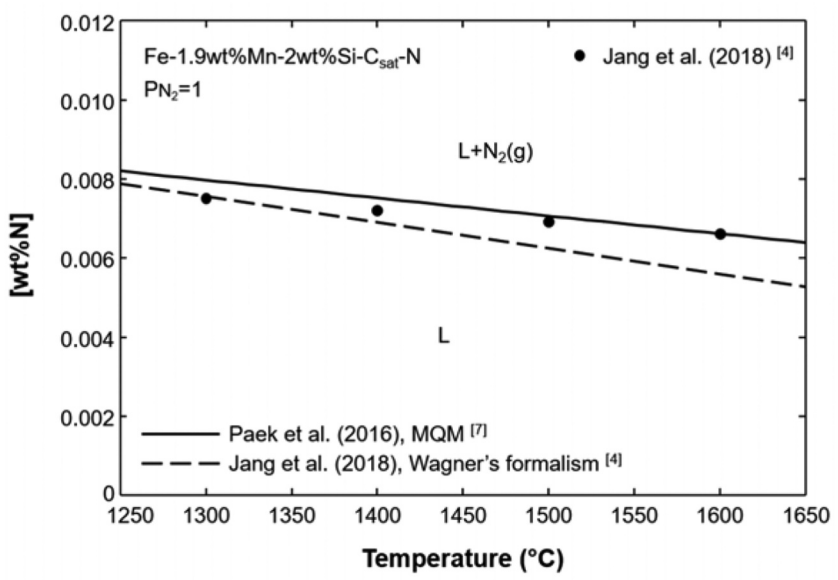

Figure 1. Temperature dependence of N solubility in Fe-1.9 wt%Mn-2 wt%Si-C_{sat} melt under 1 atm N_2 pressure along with thermodynamic calculation by Wagner's formalism (dashed line) and MQM (solid line).

The thermodynamic behaviour of N in solid phases can be predicted by the modelling of the Fe-Mn-Si-C-N system. Based on the CALculation of PHAse Diagram (CALPHAD) method, the core alloy composition of the quaternary Fe-Mn-Si-C system has been optimised recently by the present authors [8]. Later, the N behaviour in the solid solutions such as FCC and BCC phases has been added in the core system database using the Compound Energy Formalism (CEF) [9], which were recently stored in the FSStel database of FactSage thermochemistry software version 7.3 [10]. In order to check the validity of the modelling result for the carbon saturated condition of the core system, the phase transition temperature of Fe-Mn-Si-C_{sat} alloy was measured with increasing Mn content using differential scanning calorimetry. In addition, the cooling and quenching experiments were carried out to simulate the N_2gas formation reaction during solidification of the N containing Fe-Mn-Si-C_{sat} alloy. The microstructure of the samples will be compared with the cooling curve predicted by the model calculation and used for the thermodynamic analysis of the N_2gas formation at low-temperature region.

Experimental procedure

Master alloy

The carbon saturated Fe-Mn-Si alloy was melted using a 15 kW/40 kHz high-frequency induction furnace under an Ar atmosphere. 200 g of electrolytic Fe (99.99%purity) contained in a graphite crucible was heated up to 1600°C. The melt temperature was directly measured by immersing a Pt/Pt-13 wt%Rh thermocouple sheathed with an alumina tube. The liquid alloy was homogenised for 1 h to reach the C saturation condition. Then, Si shot (99.999%purity) was first added for the desired Si concentration around 3 wt%, and Mn (99.99% purity) was added repeatedly up to 4.5 wt%. After every Mn addition with 1 h of homogenisation time, the metal sample of about 10 g was extracted by a 4 mm inner diameter quartz tube connected to a syringe (10 mL). The samples were quenched rapidly in water within 2 s. The C content was analysed by the combustion method with a thermal conductive detector (Thermo Scientific, ThermoFlash Smart EA CHNS/O with MV). Si and Mn contents were analysed using the Inductively Coupled Plasma-OpticalEmission Spectroscopy (ICP-OES, Perkin Elmer Optima 7100DV). The composition of the analysed master alloy is shown in Table 1.

Differential scanning calorimeter (DSC)

The master alloys were carefully cut and polished for the DSC analysis (NETZCH STA 449 F1 Jupiter). 150 mg of the sample was charged in the alumina crucible (OD: 6.8 mm, H: 4 mm) with lid under the purified Ar gas for purge gas (20 mL/min) and protective gas (30 mL/min). Since alloying elements, Si, Mn and C in the cast iron have a strong affinity with O, the use of Ti or Zr getters utilised in the DSC chamber was not effective in

Table 1. Chemical composition of C saturated Fe alloy containing Si and Mn. (wt%).

Sample number	Si	Mn	C	Fe
#1	2.92	0	4.53	balance
#2	2.69	1.46	4.54	
#3	2.79	2.98	4.63	
#4	2.69	4.50	4.67	

preventing the oxidation of alloys at high-temperature region. In order to purify the Ar gas, the high purity Ar (purity 5.0) was passed through the silica gel and phosphorus pentoxide (P_2O_5) to remove moisture, ascarite (sodium hydroxide-coated silica) to remove CO_2, and then blown into the pre-heating resistance furnace charged with Mg wires. The Mg turning furnace was heated up to 500°C for the best oxidation conditions of Mg to consume the O_2 in the Ar gas. The oxygen potential, PO_2 of the deoxidised Ar gas reached less than 10^{-20} in atm. Under the dehydrated and deoxidised Ar atmosphere, no oxidation was observed during the analysis, which was confirmed by the constant Thermogravimetric (TG) curve. As shown in Figure 2, for example, the sample mass of Fe-1.46 wt %Mn-Si-C_{sat} alloy was changed within ±0.03% during heating and cooling. Two heating and cooling cycles were run for each sample. The temperature profile was also plotted along with the TG curve in the figure. The transition points of the samples were measured by the exothermic or endothermic reaction at the onset point of the phase transformation. The heating and cooling rate was 10°C/min.

Cooling and quenching experiment

The gas-metal equilibrium experiments were carried out to measure the N solubility of liquid and solid cast iron alloys at various temperatures using an electric resistance furnace heated by $MoSi_2$ (Nabertherm, RHTV-40) with an alumina reaction tube (OD: 46 mm, ID: 40 mm, H: 1100 mm). The temperature of the hot zone was measured by a Pt/Pt-13 wt%Rh thermocouple. Two grams of the master alloy (sample #2) were charged in a graphite crucible (OD: 15 mm, ID: 9 mm, H: 20 mm). The crucible was placed in a kanthal wire cage and suspended in the hot zone of the furnace. The temperature was kept at 1300°C under 1 atm N_2 atmosphere. The gas flow rate was controlled by a mass flow controller in the range of 100 mL/min. The alloy melt was stabilised and homogenised for 2 h. After 2 h of equilibration, the reaction temperature was lowered to 900°C, 700°C and 500°C, respectively, with the cooling rate of 10°C/s and held for 2 h at each temperature prior to quenching. The microstructure of the sample was analysed by Scanning Electron Microscopy-Energy Dispersive X-ray spectroscopy (SEM-EDS, Tescan, Mira 3).

Results and discussion

Phase transition in Fe-Mn-Si-C_{sat} alloy

The applicability of the modelling result in the Fe-Mn-Si-C system [8] was checked for the C saturated condition by comparing the calculated phase diagram of Fe-Mn-2.7 wt%Si-C (Figure 3) with the thermal analysis data using DSC. The transition temperatures of Fe-Mn-Si-C_{sat} alloys were measured by the DSC signal as shown in Figures 4 and 5.

During the heating up to 1300°C, two transitions were observed at the low temperature near the eutectoid point and high-temperature region near the melting point for all the alloy samples as shown in Figure 4. The onset points at low-temperature agreed reasonably with the phase boundary of FCC/BCC as shown in Figure 3. At the high-temperature region, the sharp peaks were observed near the melting temperature of the alloys. The onset point of such peaks corresponded very well with the solidus temperature as shown in Figure 3. The peaks of the second heating segment had two maximum points or inflection; however, it was difficult to decompose the overlapped peaks into two peaks within 10°C by

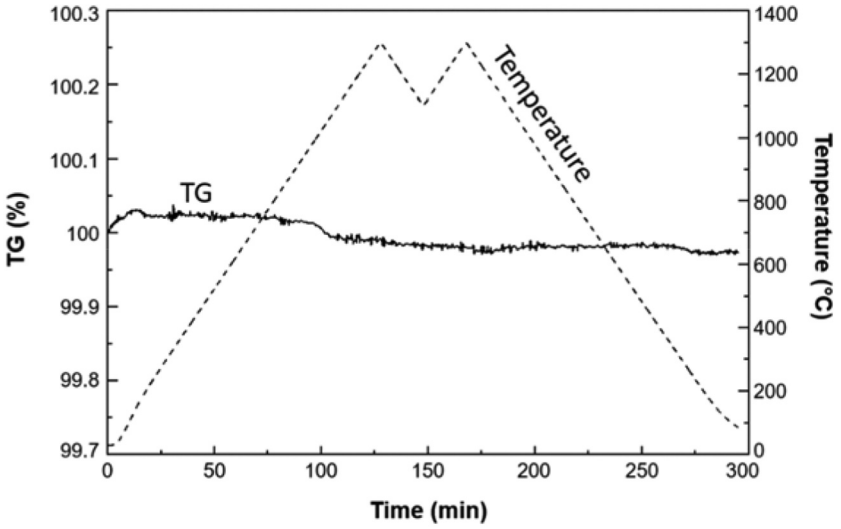

Figure 2. Temperature profile programmed for the thermal analysis (dashed line) and corresponding TG analysis under the deoxidised Ar atmosphere (solid line).

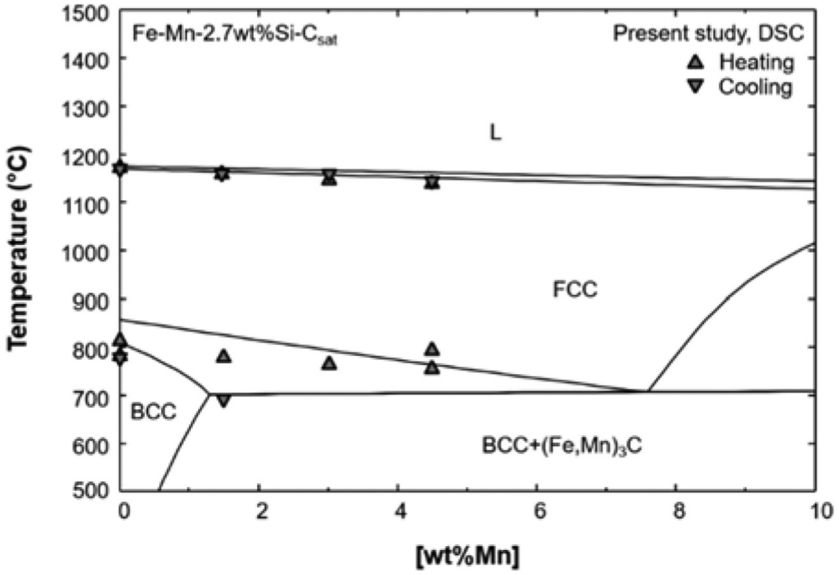

Figure 3. Calculated phase diagram of the Fe-Mn-Si-C system under the unit activity of C along with the present experimental results.

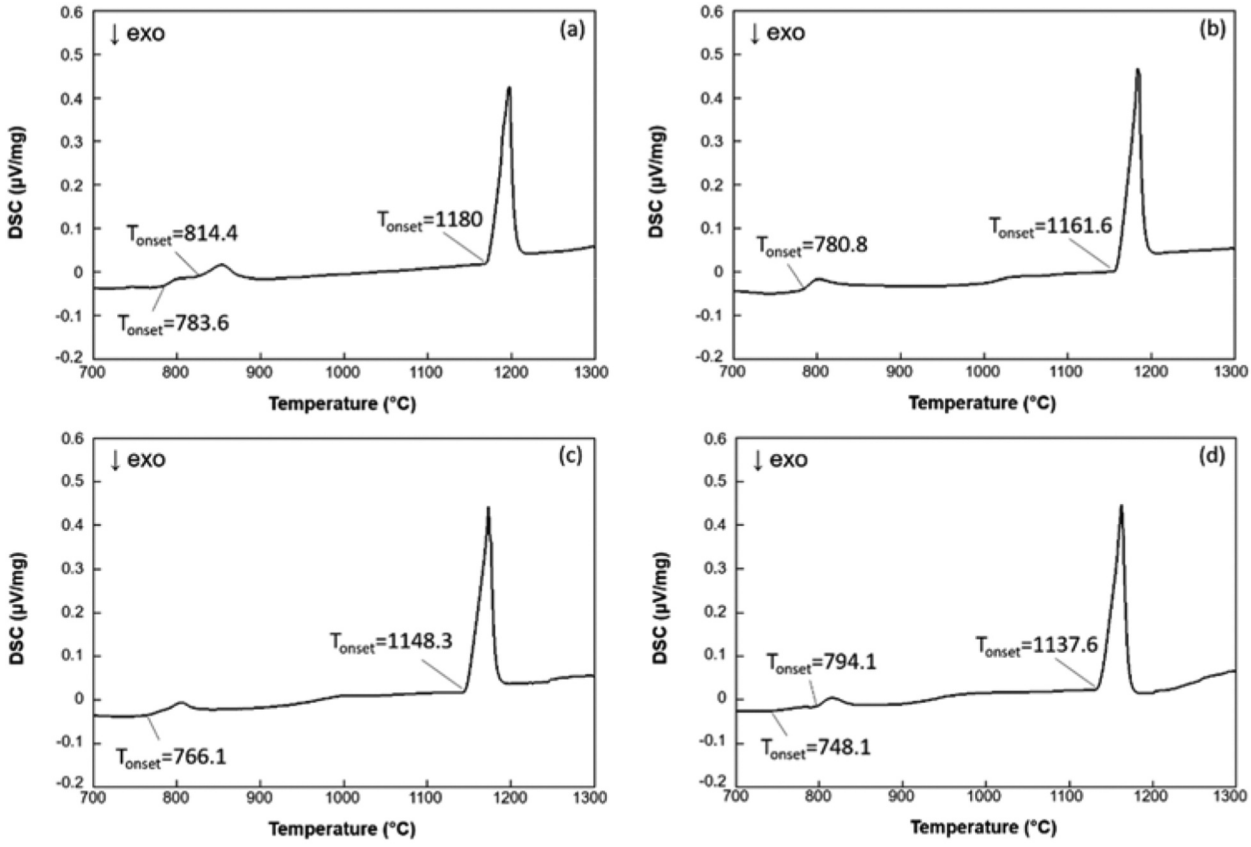

Figure 4. Thermal analysis results during heating for (a) Fe-Si-C_{sat}, (b) Fe-1.46 wt%Mn-Si-C_{sat}, (c) Fe-2.98 wt%Mn-Si-C_{sat} and (d) Fe-4.50 wt%Mn-Si-$C_{sat.}$

using a deconvolution method. This indicates that the significant enthalpy changes of both transitions of FCC/FCC+L (solidus) and FCC+L/L (liquidus) at the phase boundary of the two phase region. Therefore, only the first heating segment data were used in this study.

During cooling, the transition point at the two phase region of BCC/FCC was hardly measurable. The low-temperature transitions near the BCC/FCC phase boundary and eutectoid point were only observed at low Mn concentration as shown in Figure 5(a,b). On the other hand, the onset points of high temperature peak clearly

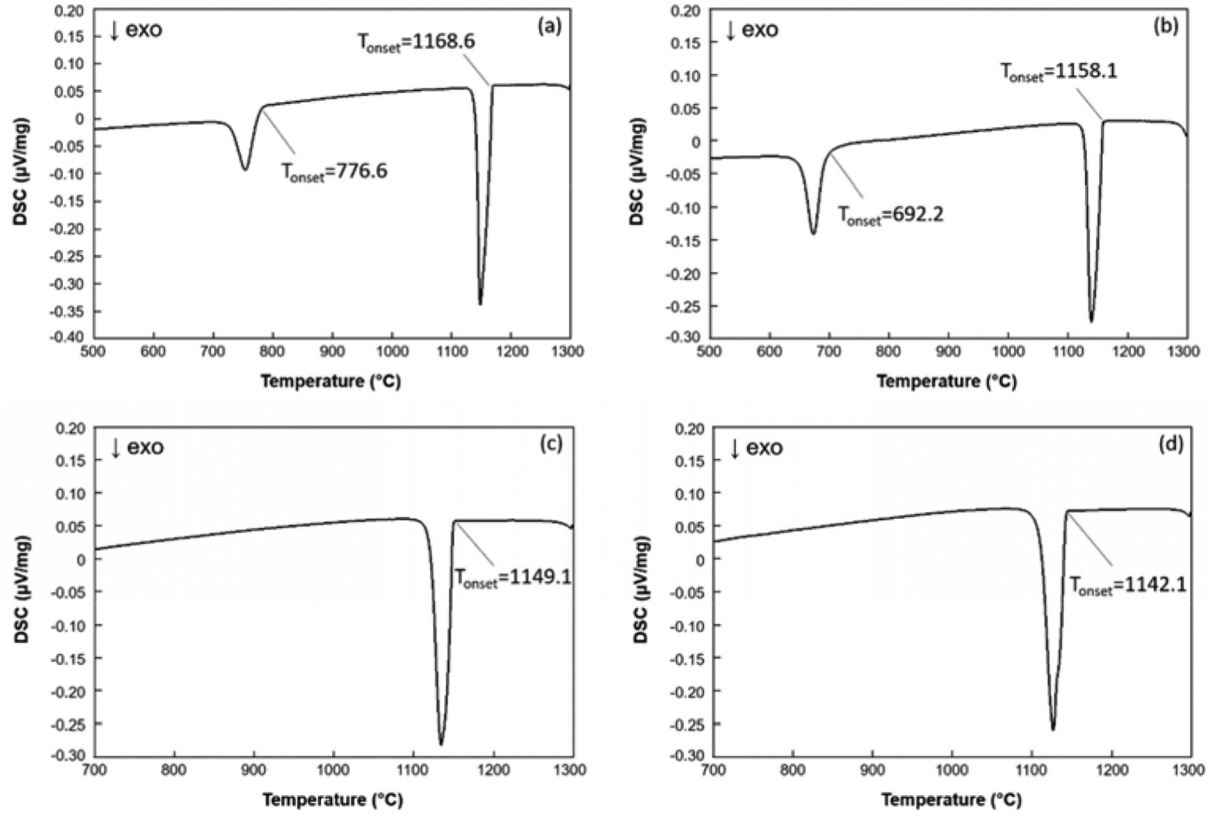

Figure 5. Thermal analysis results during cooling for (a) Fe-Si-C_{sat}, (b) Fe-1.46 wt%Mn-Si-C_{sat}, (c) Fe-2.98 wt%Mn-Si-C_{sat} and (d) Fe-4.50 wt%Mn-Si-C_{sat}.

distinguished as the sharp peaks and corresponded well with the solidus point of the Fe-Mn-Si-C phase diagram as shown in Figure 3. Even though the single minimum points were detected from the cooling curves at high temperatures, the undercooling effect cannot be completely ignored. In order to clarify the phase transition at liquidus and solidus during cooling, further research is required under the various cooling rates.

Temperature dependence of N solubility in cast iron

The solubility limit of N has a direct influence on the generation of N_2 gas during cooling and solidification of cast iron. In the liquid alloy saturated with C, the C solubility significantly increased with increasing temperature. Meanwhile, the N solubility can be decreased due to the strong repulsion force between C and N in liquid iron alloys. This has been recently confirmed experimentally [4] and theoretically [7] as shown in Figure 1. In the commercial casting process, the pouring temperature is frequently increased before casting to prevent the N defects, which reflects that the increased C equivalent decreases the N solubility in liquid cast iron. This tendency can be also described clearly by the phase diagram for the C saturated condition. Figure 6 shows the calculated phase diagram under the unit activity of C for the Fe-1.46 wt%Mn-2.69 wt%Si-C_{sat}-N alloy, and the bold line represented the N solubility of the alloy in equilibrium with atmospheric N_2 pressure. As shown in the figure, the N content in the liquid alloy decreases with increasing temperature.

The same temperature dependence of the N solubility was observed for the FCC solid solution. The N solubility in FCC decreases with increasing temperature in the temperature range below the melting temperature of the alloy. However, when the temperature is lower than a critical point, the N content decreased with lowering the temperature due to the formation of Si_3N_4 phase. In the BCC phase, the solubility product of the Si_3N_4 was further decreased at the low-temperature range due to the low capacity of soluble N in the BCC matrix.

The phase transformation and related N solubility limit were confirmed by the cooling and quenching experiments at various temperatures. The Fe-1.46 wt%Mn-2.7 wt%Si-C_{sat} alloy melt was equilibrated at 1300°C for 2 h under N_2 gas, and then the samples were quenched in water, air and furnace, respectively. **Figure 7** compares the microstructure of the samples depending on the quenching method. Only graphite flake was observed in the sample quenched in water (Figure 7(a)). However, thin and sharp defects were observed in the air-quenched sample (Figure 7(b)), and it was increased even further for the sample of furnace cooling (Figure 7(c)).

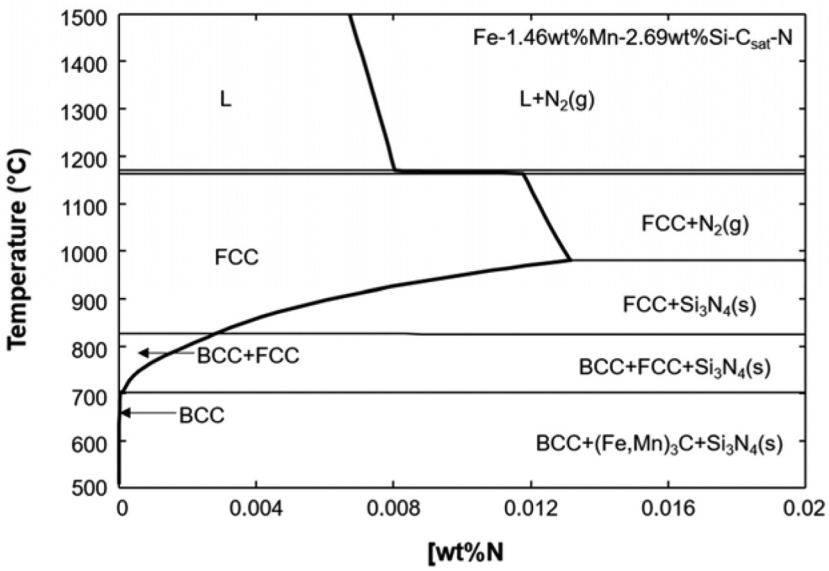

Figure 6. Calculated phase diagram of Fe-1.46 wt%Mn-2.69 wt%Si-C_{sat}-N alloy under the unit activity of C.

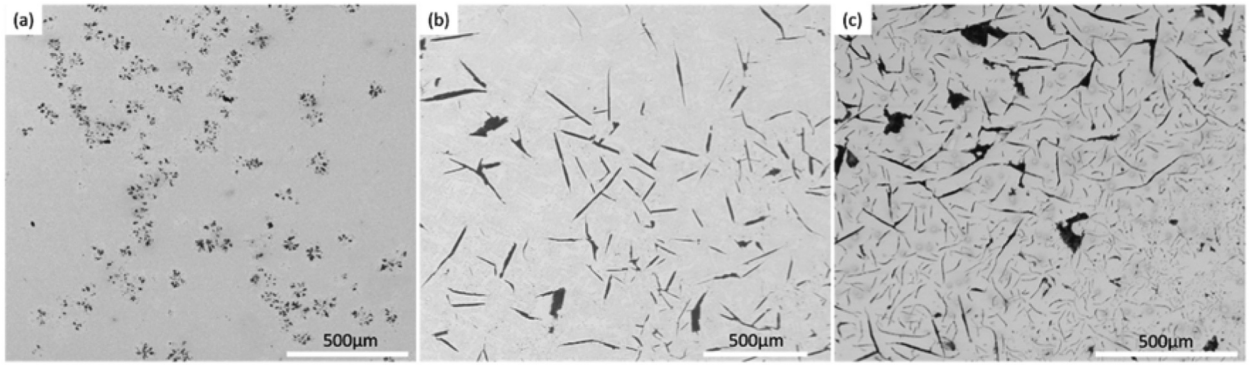

Figure 7. SEM micrograph of Fe-1.46 wt%Mn-2.69 wt%Si-C_{sat}-N alloy quenched in (a) water, (b) air and (c) furnace.

In order to confirm the effect of temperature on the N defect formation during cooling, the Fe-1.46 wt% Mn-2.69 wt%Si-C_{sat} alloy melt was cooled down from 1300°C to 900°C, 700°C and 500°C, respectively. As shown in Figure 8(a), at 900°C, the defects have formed along the graphite flakes in the FCC matrix. Below 700°C, the alloy phase can be completely transferred to BCC structure, and the N solubility limit in BCC is rapidly decreased as shown in Figure 6. Therefore, the super-saturated N in the solid solution can form the N_2gas in the BCC matrix. The micropores were detected in the middle part of Figure 8(b). Such small size of N defects have spread over the sample at 500°C as shown in Figure 8(c). The nitride phase of Si_3N_4 was not observed because the alloy cannot be fully saturated by N by the loss of N during cooling and quenching. The carbide phase of $(Fe,Mn)_3C$ was not formed in the as-cast samples under the non-equilibrium condition of the 2-h heat treatment. Even though the low-temperature equilibrium phases were not detected, the effects of temperature and

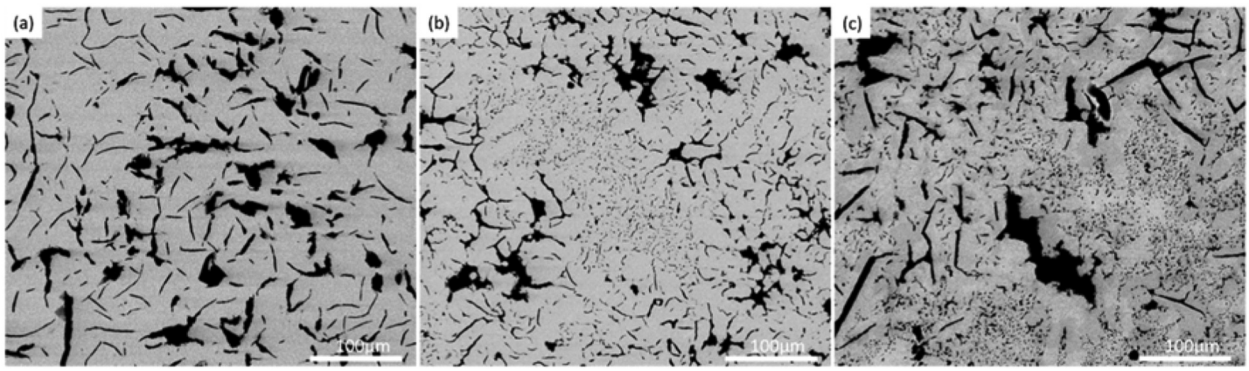

Figure 8. SEM micrograph of Fe-1.46 wt%Mn-2.69 wt%Si-C_{sat}-N alloy at (a) 900, (b) 700 and (c) 500°C.

phase transformation on the formation of N defects were simply verified by the solubility limit of N in each phase.

Summary

In the present study, the phase transition points of FCC/BCC and FCC/L in the Fe-Mn-Si-C_{sat} alloy were measured by the calorimetric method under the purified Ar atmosphere to verify the recent thermodynamic modelling result of the Fe-Mn-Si-C system. The modelling approach was also applied to describe the N defect formation during cooling and solidification of the C saturated iron alloys. The slower cooling rate has led to more N defects in the matrix of the Fe-Mn-Si-C_{sat} alloys. The number of micropores was increased with decreasing the heat treatment temperature due to the formation of the N_2 bubbles with the decreased solubility limit of N in FCC and BCC solid solutions. Therefore, the strict control of cooling rate and initial N content is required to prevent the N defects such as blowholes and micropores in the grey cast iron.

Acknowledgements

Funding from the Business Finland, SYMMET project (grant number 3891/31/2018) is greatly appreciated. This study utilized the Academy of Finland's RawMatTERS Finland Infrastructure (RAMI), based jointly at Aalto University, GTK and VTT.

Disclosure statement

No potential conflict of interest was reported by the authors.

ORCID

Min-Kyu Paek http://orcid.org/0000-0001-7933-0157
Daniel Lindberg http://orcid.org/0000-0002-8442-1237

References

[1] Laird G, Powell GLF. Solidification and solid-state transformation mechanisms in Si alloyed high-chromium white cast iron. Metall Trans A. 1993;24(4):981–988.
[2] Gundlach R, Meyer M, Winardi L. Influence of Mn and S on the properties of cast iron Part III-testing and analysis. Int J Metalcasting. 2015;9(2):69–82.
[3] Jang JM, Seo SH, Jiang M, et al. Nitrogen solubility in liquid Fe-C alloys. ISIJ Int. 2014;54(1):32–36. .
[4] Jang JM, Kim DH, Paek MK, et al. Nitrogen solubility in cast iron containing C, Si and Mn. ISIJ Int. 2018;58(7):1185–1190. .
[5] Wagner C. Thermodynamics of alloys. Cambridge, MA: Addison-Wesley Press; 1952. p. 47.
[6] Lupis CHP, Elliott JF. Generalized interaction coefficients Part I: definitions. Acta Metall. 1966;14:529–538.
[7] Paek MK, Chatterjee S, Pak JJ, et al. Thermodynamics of nitrogen in Fe-Mn-Al-Si-C alloy melts. Metall Mater Trans B. 2016;47B:1243–1262.
[8] Paek MK, Lindberg D, Kang YB, et al. Thermodynamic modeling of Fe-Mn-Si-C system, proceeding of CALPHAD XLVIII; 2019. Vol. 73; Singapore.
[9] You Z, Paek MK, Jung IH. Critical evaluation and optimization of the Fe-N, Mn-N and Fe-Mn-N systems. J Phase Equilib Diffus. 2018;29:650–677.
[10] Bale CW, Chartrand P, Decterov SA, et al. FactSage thermochemical software and databases. CALPHAD. 2009;33(2):295–311.